Research on Engineering Structures & Materials
www.jresm.org

Research Article

Internal force transfer in segmental RC structures

Seymur Bashirzade[a], Okan Ozcan[b,*], Izzet Ufuk Cagdas[c]

Department of Civil Engineering, Akdeniz University, Konyaaltı, Antalya, 07058, Türkiye

Article Info

Article history:

Received 09 Jan 2024
Accepted 06 May 2024

Keywords:

Segmental structures;
Segmental beams;
Intersegmental joints;
Hollow circular beams;
DIANA

Abstract

The primary objective of this numerical study is to provide a finite element (FE) analysis approach for segmental structures. The study was conducted using a hollow circular segmental structure model capable of adequately imitating real structural behavior and deals with the effect of varying number of segments on structural performance. In order to verify the FE procedure conducted by DIANA software, comparisons are made with the acquired numerical results and the results taken from previous experimental studies for 1 reinforced concrete (RC) beam, 2 post-tensioned (PT) beam, and 3 segmental post-tensioned beams (SPT). For the considered cases, 1D line, 2D shell, and 3D solid FE models are made, and it is found out that the 3D solid model with interface elements yields the most plausible results. Further, the FE model was constructed to accurately predict segment joint behavior concerning the relationship between the number of segments, concrete compressive strength, and the width of the openings at the segment joints up to collapse. In this study, a hollow circular segmental structure model is utilized to mimic real structural behavior, presenting a novel perspective on internal force transfer mechanisms within segmental structures. Moreover, the FE model is tailored to accurately predict segment joint behavior, elucidating the intricate relationship between the number of segments, concrete compressive strength, and the width of openings at segment joints up to collapse. In addition to presenting a robust numerical analysis framework, this study contributes novel insights into the complex interplay between segmental geometry, material properties, and structural behavior, thus advancing the state-of-the-art in segmental structural design. Thus, a modular construction methodology is proposed for segmental beam type structures ensuring safety, efficiency, and flexibility in challenging load conditions.

1. Introduction

Segmental structures, which consist of reinforced concrete (RC) segments connected by post-tensioning, can be considered as a successful approach in modern offshore construction [1] Therefore, the determination of ultimate load, displacement capacity, crack width, and locations in segmental structures becomes an important design issue which is the main motivation for this study.

Several studies have been conducted on segmented and precast underwater tunnels in which the influence of material properties [2, 3], corrosion [4], lining damage [5], joint waterproofing [6] and high-water pressure [7] on structural performance was investigated. Segmental offshore wind turbines have precast concrete segments that are established on-site and joined by external prestressing tendons, presenting a cost-effective alternative to traditional steel towers [8] In addition, the use of ultra-high-performance fiber-reinforced concrete has been combined with the segmental construction method,

*Corresponding author: ookan@akdeniz.edu.tr
[a]orcid.org/0000-0002-0870-6345; [b]orcid.org/0000-0001-9905-1657; [c]orcid.org/0000-0002-2528-2978
DOI: http://dx.doi.org/10.17515/resm2024.146st0109rs

which is a more economically and ecologically suitable alternative for offshore structures [9] Analysis and design of segmental structures is more challenging comparing with conventional RC structural design. Queiroz and Horowitz (2016) have investigated [10] the shear behavior of hollow circular segments under various loading conditions and provided insights into the practical consequences of structural design regarding the Canadian Code [11] and the Brazilian standard [12] The shear strength provided by the shear keys and either by the smooth surfaces in contact [13] or by dry joints [14, 15] has been calculated. Further, finite element (FE) models were used to analyze the stress, deformation, and damage of structures, modeling the shear strength, and opening behavior of dry joints [14] The related Spanish code provides valuable information on external prestressing method, which may be used in design [16] As can be seen from the survey so far, the literature on the design and analysis of segmental hollow circular RC structures is not extensive.

The literature review underscores the significance of recent advancements in incorporating design solutions derived from the field of wave propagation in unit cell concepts periodic structures analysis, particularly relevant to segmental (beam) structures composed of RC segments connected by post-tensioning [17] Moreover, exploration into the fracture toughness behavior of interpenetrating phase composites [18] and rate-dependent hyperplasticity with internal functions [19] present valuable insights into material behavior in periodic structures with a finite element approach [20] This research demonstrates the practical relevance of theoretical frameworks in engineering applications which contributes to the understanding of structural integrity and performance in complex systems, aligning with the objectives of analyzing segmental (beam) structures. Further, recent studies have provided insights into the structural design, testing and performance assessment of pouch cells, emphasizing the importance of material behavior [21] and geometric shape [22] in energy storage systems using finite element analysis [23, 24] under varying loading conditions.

The present study focuses on the nonlinear structural behavior of hollow circular segmental post-tensioned (SPT) beams under 4-point static bending. A scaled prototype structure is selected for the numerical study. DIANA FE software is selected as the computational tool as it has been successfully applied in RC structural analysis in previous studies found in the related literature [25-27] First, several verification problems are solved in order to gain insight into the details of DIANA software in RC structural design and comparisons are made with the experimental results presented in the cited studies. The first problem considered is a monolithic RC beam under transverse loading for which experimental results were presented. [25] 1D, 2D and 3D FE models are made and after obtaining plausible and acceptable numerical results, which are in very good agreement with the experiments, a post-tensioned (PT) beam is considered [26] Similarly, near perfect agreement with the experimental results was observed for the PT beam for all FE models. Then, experimental results presented [27] for segmental post-tensioned (SPT) beams are compared with the FE numerical results obtained and agreement was only observed for 2D and 3D models. Next, the scaled prototype structure is analyzed but only a 3D FE model is made considering the results obtained in the verification study and due to the complicated geometry. Critical parameters, such as load capacity, displacement capacity, crack patterns, crack widths, and joint opening widths are studied in detail.

In summary, while various studies have investigated the behavior of segmental structures and their applications, there remains a notable gap in the literature concerning the nonlinear structural behavior of hollow circular segmental post-tensioned (SPT) beams. Additionally, limited attention has been given to the detailed numerical analysis of scaled prototype structures using advanced FE software such as DIANA. This study seeks to address these gaps by conducting a comprehensive investigation into the nonlinear

behavior of SPT beams, utilizing a scaled prototype structure and employing DIANA FE software. By comparing numerical results with experimental data from previous studies and analyzing critical parameters such as load capacity, displacement capacity, crack patterns, crack widths, and joint opening widths, this research aims to provide valuable insights into the performance and design considerations of segmental structural applications. Moreover, the findings regarding the influence of segmental design parameters such as the number of segments and concrete strength levels on structural behavior contribute to advancing the understanding of segmental construction methodologies in engineering. Overall, this study offers a novel perspective on the structural behavior of segmental structures, highlighting the potential benefits and design considerations of segmental construction.

2. FE modeling validation

Before proceeding with the numerical analysis of SPT concrete structures, FE models for simpler RC structures created by using DIANA FE software package are validated by comparing the numerical results obtained with the experimental results found in the related literature. Three main structural elements are considered during the verification study: RC, PT concrete, and SPT concrete beams. Different loading types and failure mechanisms were investigated in these studies [25-27] For concrete and embedded reinforcement, finite element models are developed using 1D line elements, 2D elements, and 3D solid elements [28] The 1D FE model is the simplest modeling option but the 2D model includes the influences of shear and torsion, as well as the axial behavior better than the 1D model. However, the most comprehensive analysis can be made by the 3D solid element FE model, which accounts for the entire 3D response (Fig. 1). Total strain crack models are used to simulate concrete, and pushover analyses are conducted until collapse. Concrete is modeled with exponential softening in tension and Hognestad curve is adopted to simulate the compressive behavior [29] All reinforcements and prestressed tendons are modeled as embedded with adherence-slip reinforcement. The material model for steel is based on von-Mises plasticity with linear plastic hardening based on experimental properties (Fig. 2). For the numerical analysis of hollow circular segmental post-tensioned (SPT) beams under 4-point static bending, various FE models were constructed using the DIANA FEA software package. In the FE modeling process, careful consideration was given to the selection of appropriate element types and numerical parameters to ensure accurate representation of the structural behavior under loading conditions.

In the 1D FE model, beam elements (L6BEN) with 2 nodes were utilized to represent the structural members along their longitudinal axis. The 2D FE model employed shell elements (Q20SH), with a total of 4 nodes and 2 degrees of freedom (DOF) per node, capturing the structural behavior in both the longitudinal and transverse directions. The 3D FE model utilized solid elements (HX24L) to account for the complex geometry of the segmental beams, with 8 nodes and 3 DOF per node, enabling a detailed analysis of stress, deformation, and damage distribution within the structure. Both material and geometric nonlinearity were considered in the nonlinear FE analysis, incorporating realistic behavior such as plasticity, crack propagation, and large deformations. Two distinct crack models were implemented in the FE simulations: the rotating crack model and the fixed crack model. The rotating crack model allows cracks to propagate and evolve freely within the structure, simulating the progressive failure behavior of the segmental beams. In contrast, the fixed crack model assumes predefined crack patterns and locations, providing a simplified representation of crack behavior for comparative analysis.

To ensure the accuracy and reliability of the FE simulations, stringent convergence criteria were applied during the modeling process. Convergence was assessed by monitoring key output parameters, such as displacement and stress distributions, and adjusting the FE

mesh density iteratively until stable and consistent results were achieved. A series of FE meshes were generated and analyzed, with refinement applied in regions of high stress concentration or discontinuity to capture localized effects accurately. The boundary conditions (BC) of the FE models played a crucial role in simulating realistic loading conditions and structural response. Boundary conditions, such as pinned supports, roller supports, and applied loads, were imposed to replicate the experimental setup and loading configuration. The rationale behind the BC choice was based on the physical constraints of the prototype structure and the desired response characteristics. Additionally, boundary conditions were imposed to simulate the behavior of rotating crack and fixed crack models, ensuring alignment with experimental observations. Validation of the FE models was conducted by comparing numerical results with experimental data from previous studies, including load-displacement curves, crack patterns, and failure modes. The accuracy achieved in the FE model validation process provides confidence in the reliability of the numerical simulations, enhancing the credibility of the study findings and their applicability to real-world engineering scenarios.

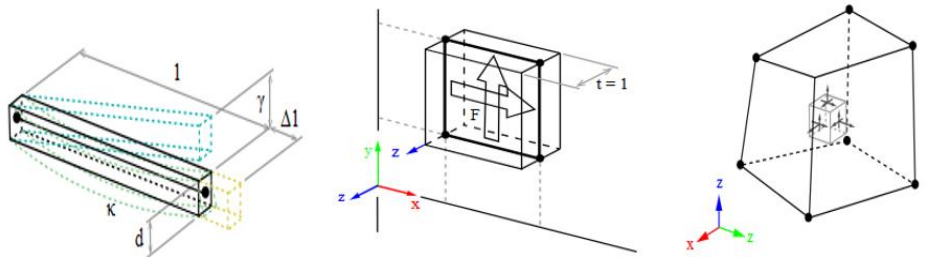

(a) b) c)

Fig. 1. DIANA element models: (a) 1D line, (b) 2D shell, and (c) 3D solid element. [28]

Pushover analyses are conducted by incrementally applying the point loads until failure in order to capture the post-peak response of the beams while providing both numerical stability and efficiency. The load increment is taken in a range between 1.0 and 3.7 kN depending on the ultimate load applied. Arc length control using the updated normal plane approach, which incorporates automated scaling of the load increment with the maximum equilibrium iteration number set equal to 25, is used to track the response path. The equilibrium iteration approach uses the secant (Quasi-Newton) method to achieve computational stability. In addition, the default parameters are used in the line search method as no significant convergence problem occurred using the default parameters. Convergence analyses of the mesh were conducted for all beams utilizing displacement measurements. The elements were meshed employing an approximate element size of 50 mm in the longitudinal and thickness directions, correspondingly.

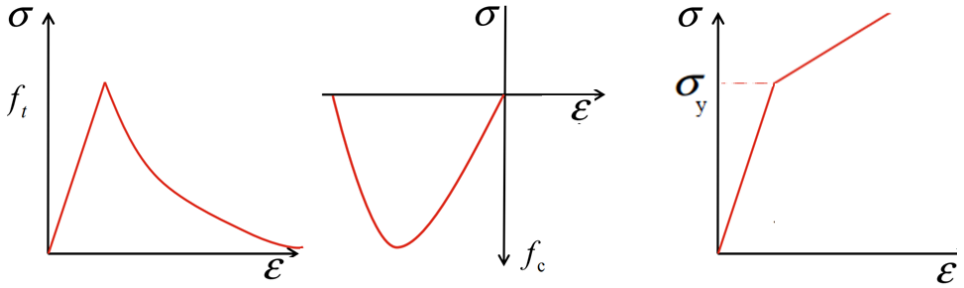

(a) (b) (c)

Fig. 2. Concrete tension (a), compression (b) and steel model (c) [30]

2.1 Comparison with RC Beam Tests

Jason et al. (2013) have investigated the cracking behavior of RC beams both numerically and experimentally [25] Four-point-bending tests were conducted on 2.85 m long RC beams with a depth of 0.25 m and a web thickness of 0.15 m. The 28-day compressive strength of concrete was 39 MPa and the steel reinforcement had yield and ultimate strengths of 550 and 666 MPa, respectively. The compression reinforcement had a diameter of 12 mm, whereas the tensile and transverse reinforcements had a diameter of 8 mm. The experimental load-displacement responses are compared with the numerical results obtained from the 1D, 2D, and 3D element models to assess the correctness and dependability of the numerical models in reflecting the complex behavior of RC beams (Fig. 1).

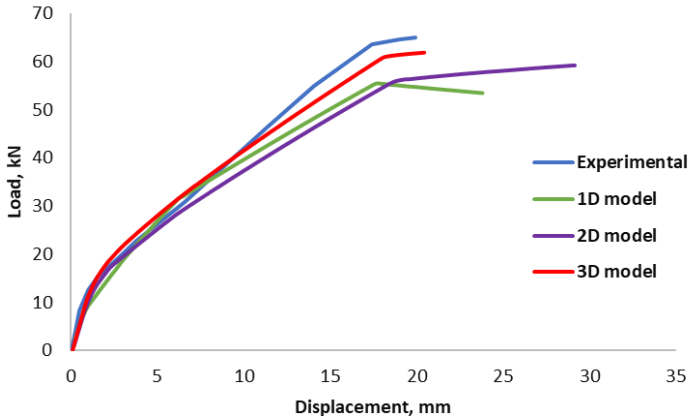

Fig. 3. Load-displacement curves of RC beam [25]

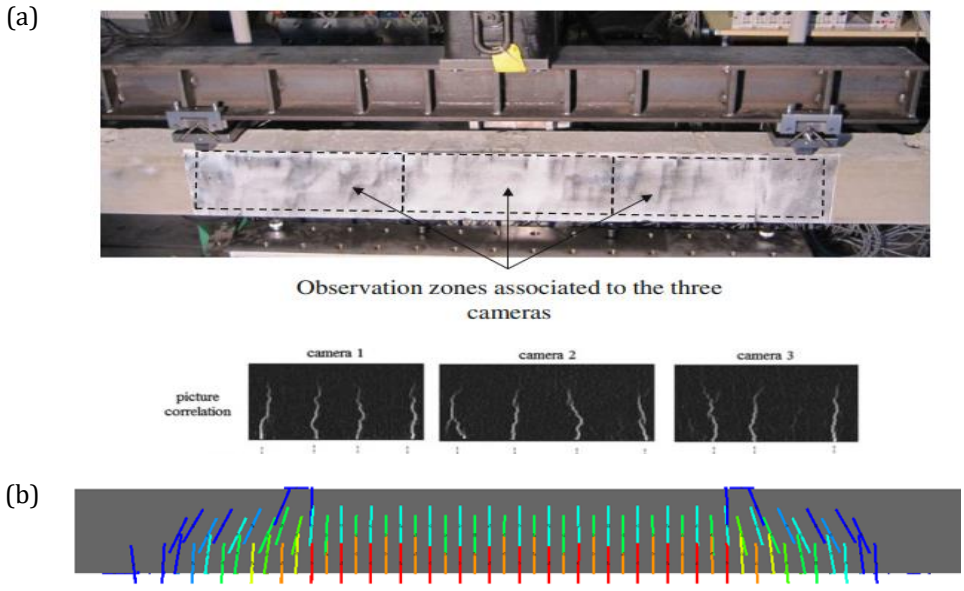

Fig. 4. Crack distribution at failure in the (a) experimental and (b) numerical model of RC beam [25]

The rotating crack model is used in the FE models and interface mechanisms are employed between the loading plates and the concrete beam. As can be observed from Figure 3, there is a very good level of agreement between the experimental and numerical initial stiffness, strength, and post-peak behavior indicating the adequacy of the numerical models to predict the nonlinear response of the RC beam. This confirms the accuracy of the FE models to capture the cracking behavior of the beams (Fig. 4).

With the establishment of an ideal correlation, the conclusive count of cracks corresponds accurately, amounting to 13 discernible cracks. It is noteworthy that the experimental initiation of cracking manifests more promptly compared to its simulated counterpart. A commendable concordance is achieved between the experimental observations and numerical simulations, particularly evident during the onset of active cracking in the initial loading phase. In the FE analysis results, a nuanced depiction is provided through various color representations, detailing the alteration in crack width along the length of the beam. Specifically, cracks depicted in red and orange colors closely resemble experimental crack locations and widths. Conversely, cracks represented in blue, green, and yellow are categorized as hairline cracks in the FE analysis, generally exhibiting widths smaller than 0.5 mm.

2.2 Comparison with PT Beam Tests

Tao and Du (1985) have investigated the flexural strength of partly PT beams with bonded and unbonded tendons [26] In the mentioned study, twenty-two unbonded and four bonded PT beams were tested for which the parameters included the loading type, non-prestressed reinforcement ratio, prestressed reinforcement ratio, and span-height ratio. For the considered beam (i.e., A9 beam in the cited reference), the concrete had a 28-day compressive strength of 33.1 MPa and the unbonded tendon prestress level after the loss was 920 MPa. The area of the non-prestressed reinforcement was 804 mm2, which contributed to the total tensile strength of the beams.

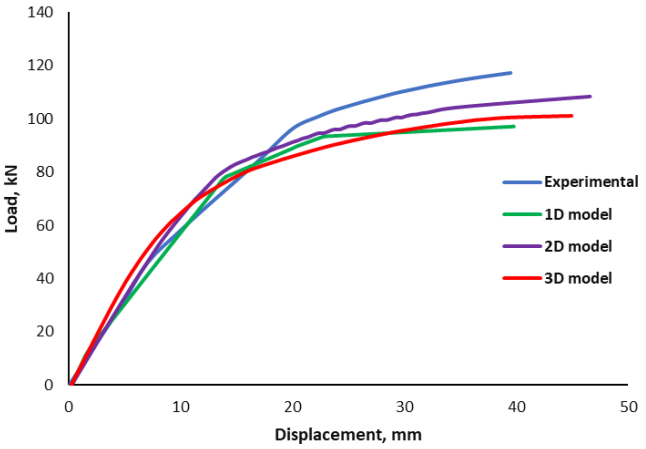

Fig. 5. Load-displacement curves of PT beam [26]

The yield strength of the prestressed and non-prestressed reinforcement was 1108 and 395 MPa, respectively. To numerically obtain the load-displacement behavior, FE models are made using 1D, 2D, and 3D elements and bar elements are used to represent the PT tendon and non-prestressed reinforcement. The analysis of PT beams using aforementioned modeling approach provides significant details on the load-displacement behavior as well as crack initiation and propagation processes. When the experimentally

obtained load-displacement data was compared to the numerical simulations, a high degree of agreement was observed, verifying the reliability and precision of the numerical models in presenting the PT beam behavior (Fig. 5). An approximate linear relationship between the applied load and displacement was observed in the early linear-elastic range while the load-displacement curves demonstrated the nonlinearity showing the deterioration of flexural capacity. The numerical models accurately predicted the load levels at which cracks occurred and propagated throughout the beam since the crack propagation sites and patterns of the experimental and numerical simulations were similar, confirming the accuracy of FE model to accurately represent cracking behavior. In the experimental investigation of the beam, notable observations indicate the prevalence of larger cracks within the central regions of the beam. However, it is discerned that variations in crack thickness led to a stratification of crack widths, delineating them as distinct entities in the FE analysis results, where the cracks are differentiated based on their magnitudes into categories denoted by blue and light blue colors. The obtained results underscore the nuanced representation of crack propagation and distribution achieved through computational modeling (Fig. 6).

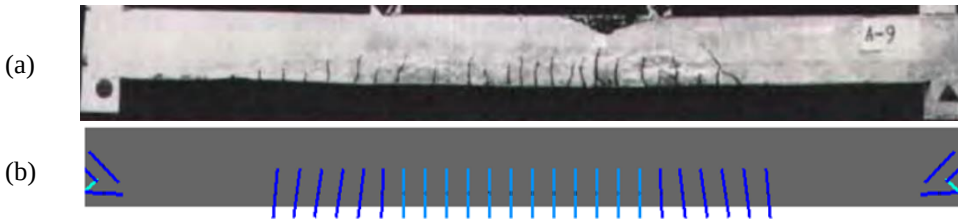

Fig. 6. Crack distribution at failure in the (a) experimental and (b) numerical model of PT beam [26]

2.3 Comparison with Precast SPT beam tests

Al-Sherrawi et al. (2018) conducted an experimental investigation on the behavior of precast SPT beams with various types of epoxy-bonded joints under static loads [27] The purpose of this study was to investigate the effects of joint shape, epoxy strength, and prestressing force on the structural performance of segmental beams and to compare the results to those of a monolithic cast beam as a reference. The compressive and tensile strength of concrete was 41.3 and 4.2 MPa, respectively. Tension reinforcement with 12 mm diameter was tied by 10 mm diameter stirrups and the post-tension tendon is made up of four 15.4 mm bars. Coulomb friction coupling was accepted at the segment joints. The MC90 mathematical formulations were used to calculate the normal and shear stiffness values based on the material parameters which are essential to evaluate the behavior and strength of the segment joints [31, 32]The reinforcement yield strength was 555 MPa and the tendons had yield and ultimate strength of 1680 and 1860 MPa, respectively.

(a)

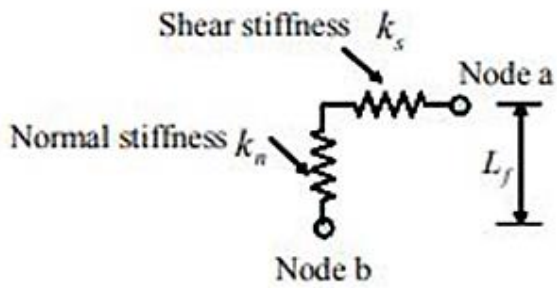

(b)

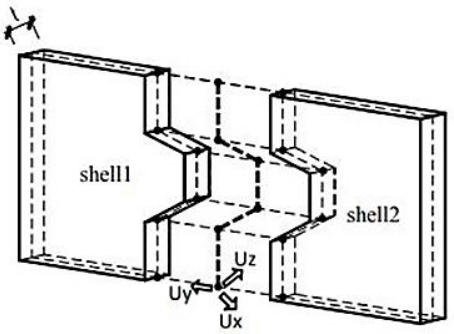

(c)

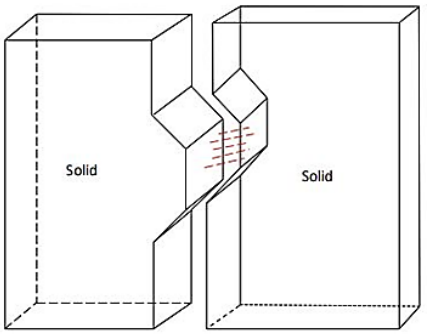

Fig. 7. Segmental interface models: (a) Joint stiffness, (b) 2D, and (c) 3D [28]

Since the segmental beams are joined from node to node, the local axis of the interface element placed at the point of intersection of the beams extended along the path direction to which the two lines and two areas joined (Figs. 7a-7c).

DIANA's structural interface components proved particularly helpful for simulating geometric discontinuities such as discrete cracks in concrete and masonry, as well as bond-slip layers in RC [28] As given in Equation 1, material models for interface elements provide a linear or nonlinear relationship between tractions, stresses, and relative displacements across the interface in which normal tractions and shear tractions $\boldsymbol{t_n}, \boldsymbol{t_t}$ are used. The relative displacements are the normal relative displacement $\boldsymbol{u_n}$ and shear relative displacement $\boldsymbol{u_t}$. In the related literature, stiffness values $\boldsymbol{k_n}$ and $\boldsymbol{k_t}$ are assigned between the segments to assure intersegmental integrity [28, 31-34] These stiffness values are defined below,

$$\begin{Bmatrix} t_n \\ t_t \end{Bmatrix} = \begin{bmatrix} k_n & 0 \\ 0 & k_t \end{bmatrix} \begin{Bmatrix} \Delta u_n \\ dt \end{Bmatrix} \tag{1}$$

$$k_n = \frac{E}{t}, k_t = \frac{G}{t} \tag{2}$$

$$k_n = \frac{E + E_{ep}}{t}, k_t = \frac{G + G_{ep}}{t} \tag{3}$$

where, Δu_n and dt denote the axial and transverse displacement components at the segment interface, respectively. E, E_{ep} and G, G_{ep} are the elasticity and shear moduli for concrete and epoxy. Cohesion in the model accounts for the adhesive forces present in the joint, which might affect the overall joint behavior. To achieve a durable and stable joint, author has used a high-strength epoxy resin to join the segments, which plays an essential role in structural integrity and load transmission. The elasticity, and shear moduli and

compressive, and tensile strength of epoxy are important elements in defining the mechanical performance of the joints. The contribution of epoxy can be considered by adding the elasticity and shear moduli of epoxy to Equation 2 as given in Equation 3. The interface components modeling the joints at the top and bottom flanges are assigned by using a Coulomb-type friction law including cohesion term c. The Breen formula [15, 35] predicts the specified values of the joint strength components, such as cohesion and friction coefficients (μ_1 and μ_2) as given below.

$$\mu_1 = 0.6, \mu_2 = 0.205\sqrt{f_c}, c = 0.996\sqrt{f_c} \quad (4)$$

The results obtained using DIANA software show that only the 2D and 3D models yield results that are in fairly good agreement with the experimental data (Figs. 8a-8d). However, it was determined that the 1D model fails to model SPT beam as the intersegmental stiffness values could not be incorporated in the 1D model.

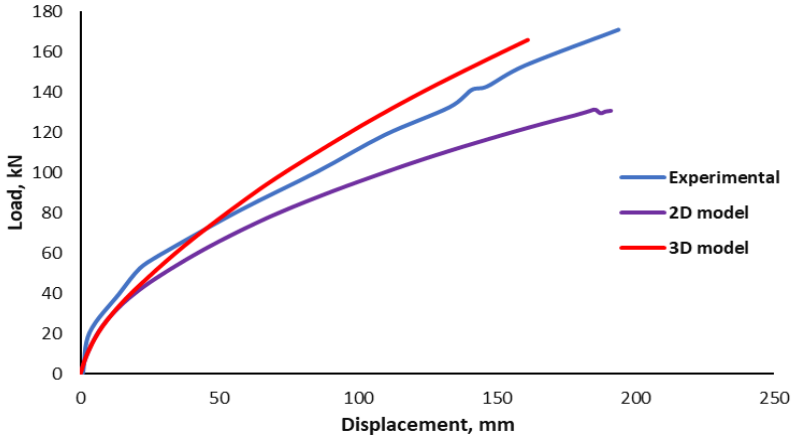

(a)

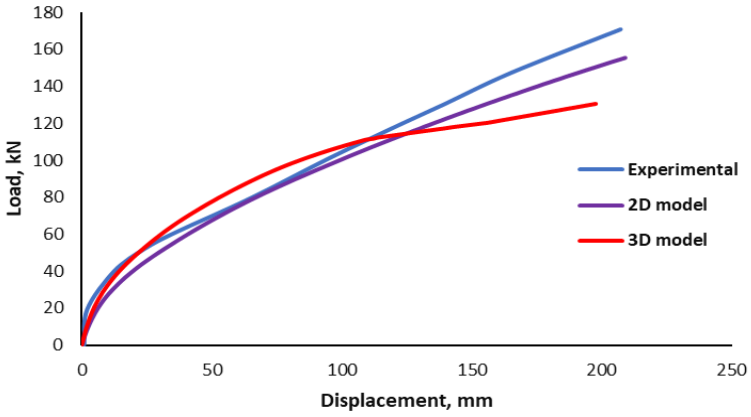

(b)

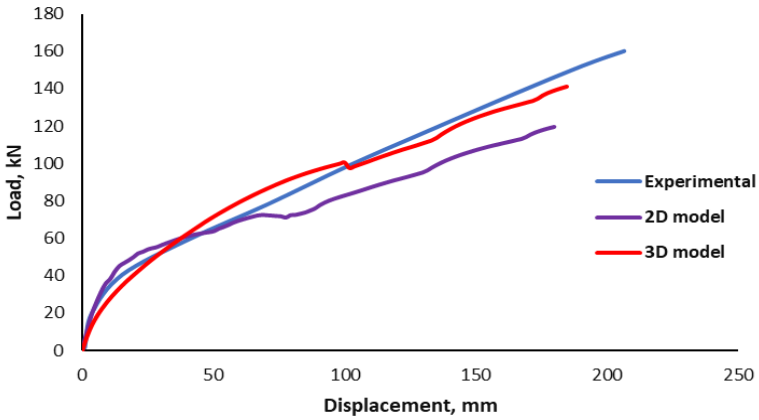

(c)

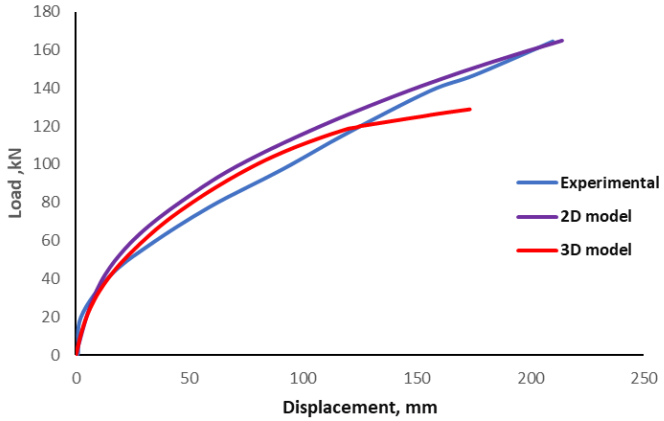

(d)

Fig. 8. Load - displacement curves of SPT beams (a) Beam (G1), (b) Beam (G2), (c) Beam (G3), (d) Beam (G4). [27]

The cracks distribution at failure shown in Figure 9 obtained using both the 2D and 3D FE models is in good agreement with the real crack distribution presented by Al-Sherrawi et al. (2018). [27] In the examination of segmental beams, it is evident that the widest cracks that occur predominantly at the segmental joints, are identifiable by a distinct red color. Conversely, as one moves away from these joints, there is a discernible shift in both the width and color of the cracks. Remarkably, the established alignment between the experimental observations and numerical simulations, is particularly pronounced during the initial loading phase where crack initiation is observed. Specifically, cracks depicted in red and orange closely mirror the experimental counterparts in terms of both location and width. In contrast, cracks depicted in shades of blue, green, and yellow define the hairline cracks in the FE analysis, typically exhibiting widths below the 0.5 mm.

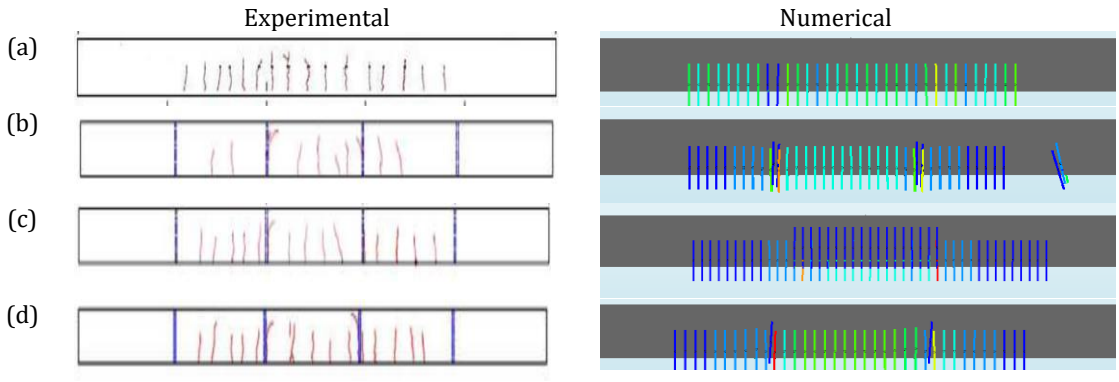

Fig. 9. Crack distribution at failure in the numerical model SPT beams: (a) Beam (G1), (b) Beam (G2), (c) Beam (G3), (d) Beam (G4) [27]

3. Parametric Study

In this section, SPT hollow circular beams are numerically analyzed by using DIANA software based on the research findings obtained from the verification study. The material models and the joint stiffness evaluation techniques for RC, PT, and SPT beam problems considered in Section 2 are directly incorporated into the FE models used here.

3.1 SPT Hollow Circular Beam

Reliable modeling of real structural behavior using numerical models is critical to produce accurate and relevant findings. Thus, the moment to shear force ratio in numerical models should be selected accordingly to achieve an exact approximation of the real structural performance. For slender structures such as offshore platform supports, wind turbine towers, and tunnels ratio becomes extremely high and therefore the influence of shear becomes insignificant as compared to bending moment. Thus, a beam under four-point-bending loads is analyzed as the ratio at the mid-span of the beam is infinite. Considering a scale factor of 10, the hollow circular beams analyzed are 10 m long with an external diameter of 1 m and an internal diameter of 0.8 m, since the selected prototype circular hollow structure is 50 m high with external and internal diameters ranging between 8-12 and 8-10 m, respectively (Table 1). Accordingly, the length of the middle span of the beam is 5 m and is divided into 1 to 5 equaling segments. The mechanical properties of the materials used in the hollow circular SPT beams are given in Table 2. The FE model details for the concrete, reinforcement, tendons, and segmental joints are shown in Figures 10a-10d.

Table 1. Geometric properties of prototype and model

	Length	External diameter	Internal diameter	Height of segments (number of segments)				
	m							
Prototype	50	8-12	8-10	10 (5)	12,5 (4)	16.67 (3)	25 (2)	50 (1)
Model	5	1	0.8	1 (5)	1.25 (4)	1.67 (3)	2.5 (2)	5 (1)

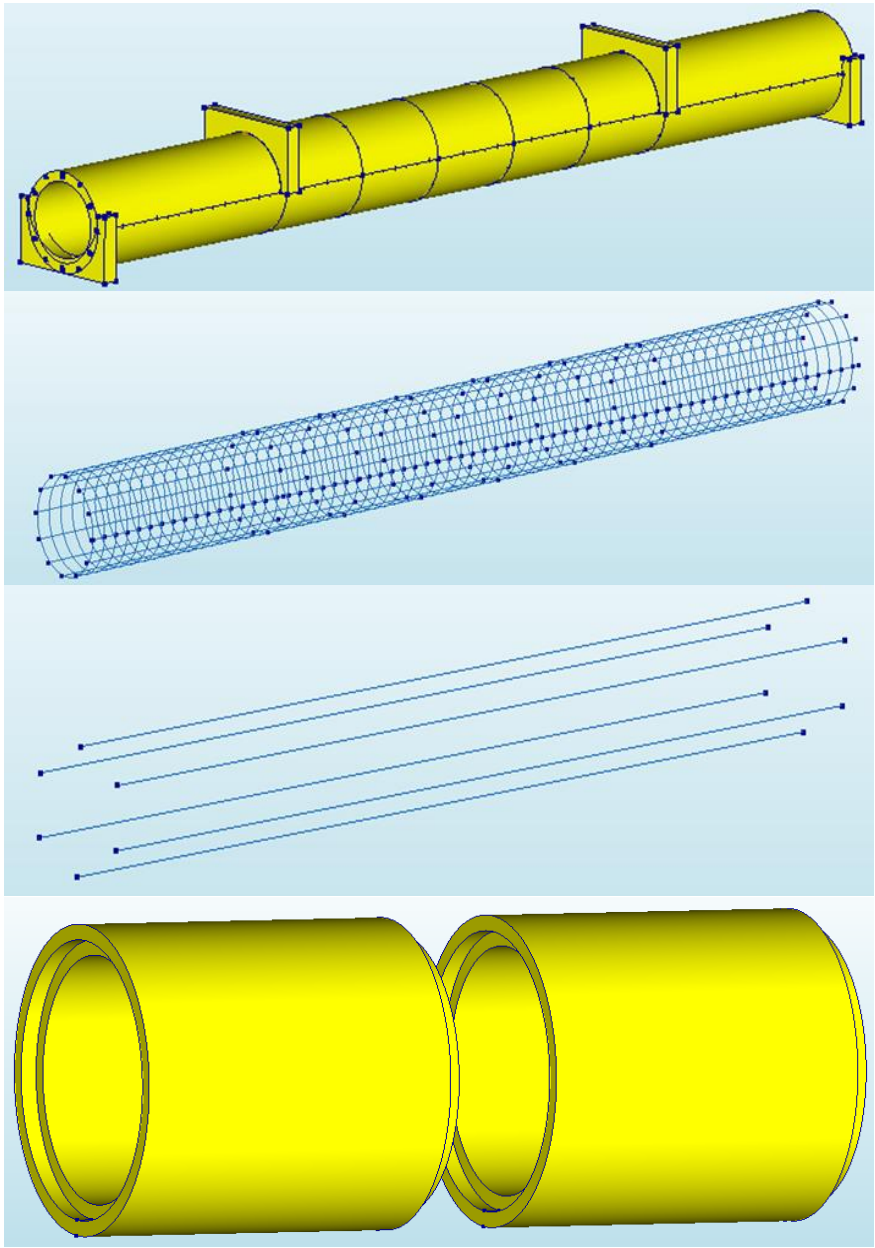

Fig. 10. The FE model of circular hollow SPT beams: (a) circular beam with support and loading plates, (b) Longitudinal and hooped reinforcements, and (c) post-tensioned tendons, (d) segmental joint details

Throughout the numerical simulation, solid elements are used to represent the concrete material, steel-bearing supports, and the reinforcements are modeled using 1D line elements. Steel reinforcements were separately modeled within each segment of the hollow circular beam. PT reinforcement enables end-to-end segments work together. Cohesive bonding is created by employing the "embedded" keyword in the DIANA software to accurately represent the interaction between the reinforcements and the concrete material.

Table 2. Materials and design parameters of numerical model.

Materials	Parameter	Value
Concrete	Elasticity modulus E	30 GPa
	Poisson's ratio ν	0.2
	Concrete compressive strength f_c	40 MPa
	Concrete tensile strength f_t	4.1 MPa
	Density ρ	2500 kg/m^3
Reinforcement	Diameter of longitudinal bar D	12 mm
	Diameter of hooped bar d	10 mm
	Elasticity modulus E	200 GPa
	Yielding strength f_{ym}	555 MPa
	Ultimate strength f_{um}	676 MPa
	Ultimate strain ε_{su}	0.02
Prestress tendon	Diameter of tendon D_f	6×15.4 mm
	Elasticity modulus E	200 GPa
	Yielding strength f_{ym}	1680 MPa
	Ultimate strength f_{um}	1860 MPa
	Ultimate strain ε_{su}	0.02

3.2 Shear Strength of Hollow Circular Section and Segmental Joints

In order to prevent premature failure of the beam at the joints before reaching maximum capacity, the shear capacity of the joints must be greater than the capacity of the beam cross section. The cross-section shear capacity is calculated as 2058.5 kN using the analytical expression provided by Queiroz and Horowitz (2016) for hollow circular cross-sections [10] The segmental joints shear capacity depends on the strength and the geometric features which directly influence the total shear capacity of the structure. For the purpose of determining the shear capacity of segmental joints and the post-tension load, the analytical expressions taken from previous studies [13-16] are used (Table 3). The expressions are based on the shear capacities of the sections and the joints considering the contributions of longitudinal compressive, normal, and shear stresses. In the analyses, the post-tensioning force is taken as equal to 1500 kN and the shear capacity of the segmental joint is calculated using the expressions given in Table 3. The shear capacity of the joint is determined to be between 2062.3 and 3492.9 kN which exceeds 2058.5 kN, the cross-section shear capacity.

Table 3. Shear capacities of section and joints

Cross-section shear capacity		
Queiroz and Horowitz, 2016	$V_c = 0.27 \cdot \alpha_{w2} \cdot \alpha_{cv} \cdot f_{cd} \cdot b_w \cdot d$	2058.5 kN
Segmental joint shear capacity		
AASHTO, 1999	$V_n = A_k\sqrt{f_{ck}}(0.2048\sigma_n + 0.9961) + 0.6A_{sm}\sigma_n$	3492.9 kN
Turmo et al., 2006	$V_n = A_k \frac{\sqrt[3]{f_{ck}^2}}{100}(7\sigma_n + 33) + 0.6A_{sm}\sigma_n$	2304.4 kN

Rombach et al., 2004	$V_n = A_k f_{ck} + 0.65 A_j \sigma_n$	2628.5 kN
ATEP, 2009	$V_n = A_j(1.14\sigma_n + 0.0564\sqrt{f_{cd}})$	2062.3 kN

3.3 Segmental Joint FE Model

The joint was numerically modeled using face-to-face interface elements having stiffness parameters based on their geometry. The elastic behavior of the interface elements is identified by the normal and tangential stiffness coefficients (k_n and k_t) in the joint model. These coefficients establish a relationship between the normal and tangential stresses (t_n and t_t) of the joint and the corresponding normal and tangential relative displacements (u_n and u_t). DIANA software automatically sets initial values to k_n and k_t to correctly recreate the initial continuous geometry before decompression. Equations 1 and 2 are used to obtain the stiffness values as was done for the SPT verification problem solved in Section 2.3. To represent the interaction between segments, a Coulomb-type friction law with cohesion given in Equation 4 is used, which is frequently applied to simulate the mechanical behavior of contact surfaces between moving segments.

3.4 DIANA Nonlinear Analysis Stage

The hollow circular SPT beam is subjected to incremental point loads until collapse. The same solid modeling approach used for the SPT beam verification problem solved in Section 2.3. is used to determine the load-displacement behavior. To prevent divergence due to large load step, the point loads are applied with an increment of 2.8 kN. As was done in Section 2., the arc length method is used without changing the related parameters. In order to examine the cracking behavior and acquire the crack widths, rotating and fixed crack models are implemented in the FE model. The rotating crack model represents a more realistic description in which cracks can grow and develop under loading conditions, whereas the fixed cracked model represents a situation in which cracks are assumed to be fixed in position with no opening or closing during the analysis.

4. Numerical Results and Discussion

Pushover analyses of 10 m long hollow circular SPT beams are conducted using the DIANA software. The 5 m long mid-section of the beams where there is no shear force are segmental and this region is divided into 1 to 5 segments. The prototype and model geometric properties are presented in Table 1. Concrete compressive strengths ranging from 20 to 100 MPa are used regarding the model with 5 segments.

4.1 Load–Displacement Relationship

The load-displacement curves of segmental beams subjected to four-point loading are shown in Figures 11a and 11b. The displacement presented are the bottom face maximum values. It can be observed from Figures 11a and 11b that for all beams, at a load level of approximately 120 kN, gaps occur at the bottom faces of segment joints and the overall beam stiffness deteriorates significantly. This probably is because at this load level the compressive stresses produced by the tendon prestress are exceeded by the tensile stresses caused by bending of the beam.

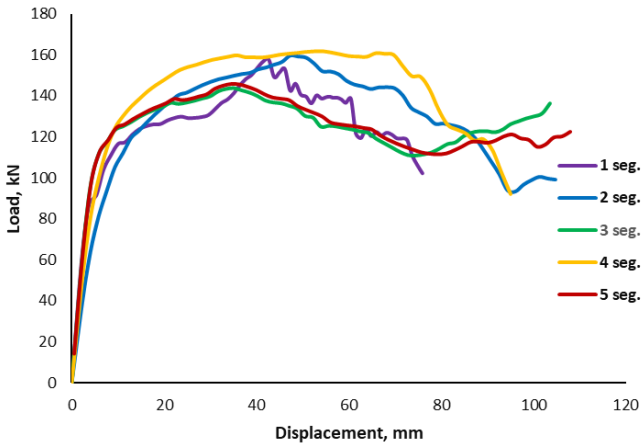

(a)

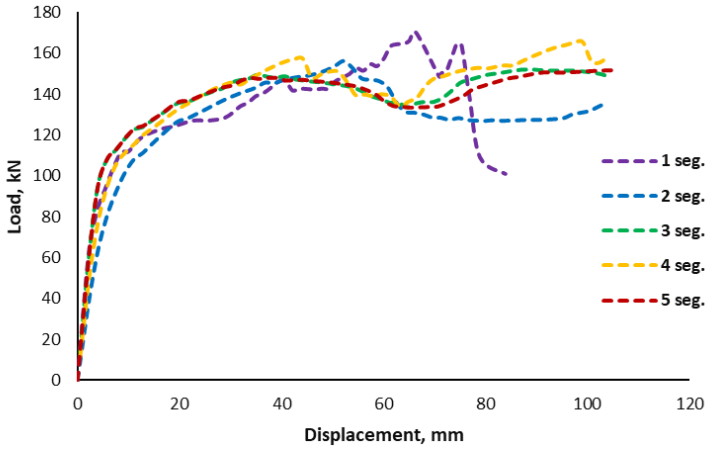

(b)

Fig. 11. Load–displacement curve of post tensioned circular hollow segmental beam: (a) Rotating crack model and (b) Fixed crack model

New gap openings no longer developed up to failure which corresponds to the load step at which convergence is no longer satisfied and the ultimate load is about 150 kN for all the beams considered. The beams collapsed at a vertical displacement of approximately 80-85 mm for the 1-segment beam and approximately 100 mm for the multi-segment beams. This observation means that the increase of the total number of segments improves ductility. Comparison of Figures 11a and 11b shows that the load-displacement behavior is similar for both crack models.

4.2 Intersegmental Joint Opening and Cracking

Comparison of Figures 11a and 11b shows that the load-displacement curves obtained using both crack models are similar. Therefore, only the rotating crack model results are presented for crack patterns. Crack distribution and joint openings are shown in Figures 12a-12d for 1 to 4 segment beams for the ultimate load stage. The crack propagation for 4 loading stages is given only for the 5-segment beam in Figures 13a-13d since similar

patterns were observed for the 1 to 4 segment beams. Herein, the crack patterns and propagation of cracks at successive load stages obtained using the FE model are consistent and physically acceptable as well.

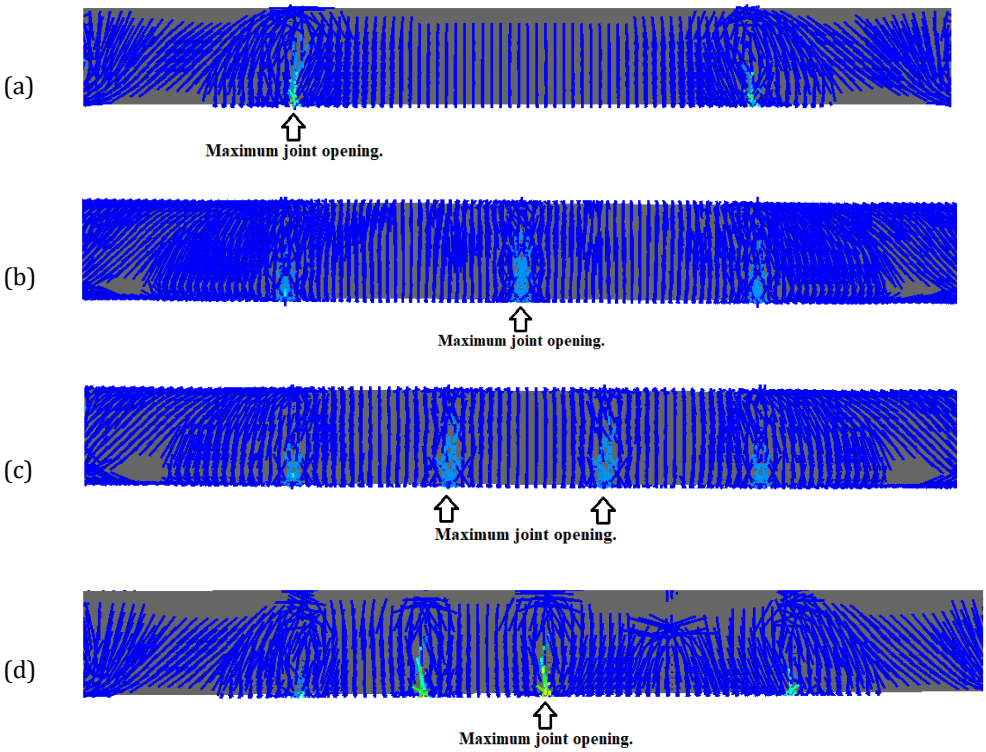

Fig. 12 Crack distribution and joint openings of hollow circular SPT beams for the ultimate load stage: (a) 1-segment beam, (b) 2-segment beam, (c) 3-segment beam, (d) 4-segment beam

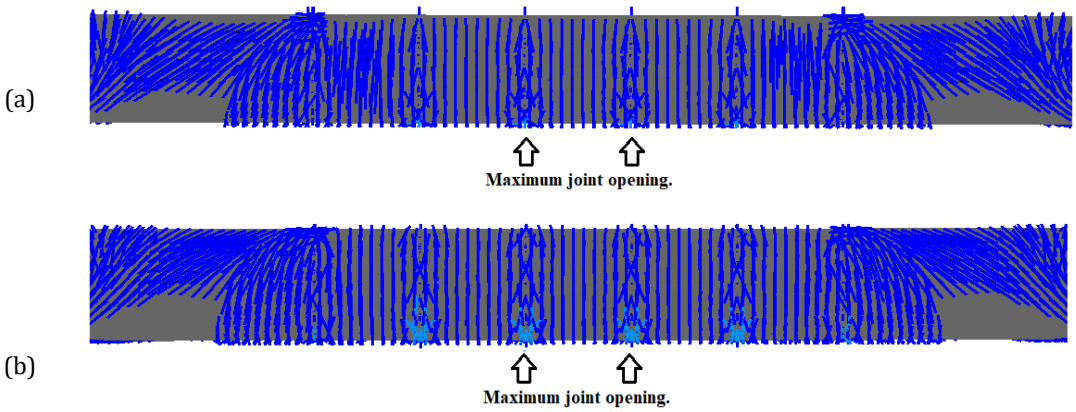

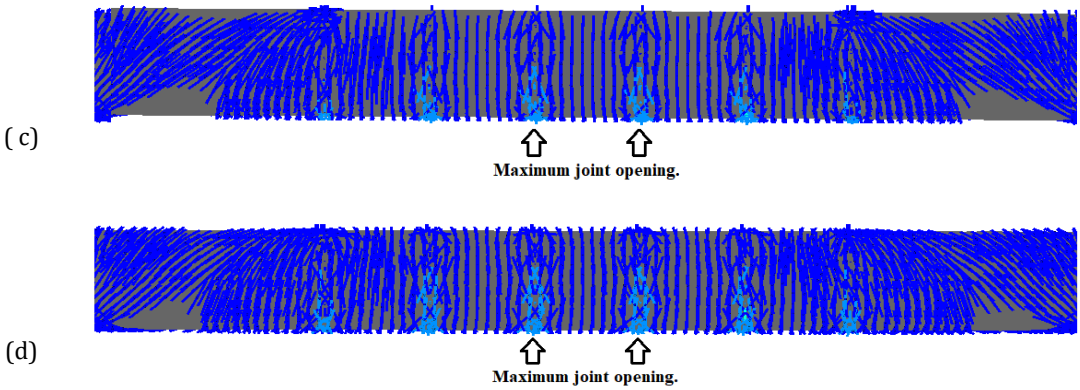

Fig. 13. Crack distribution and joint openings of hollow circular PT 5-segment beam for different load stage: (a) Load stage=0.25, (b) load stage =0.5, (c) load stage =0.75, (d) load stage =1

Figures 14a and 14b show the maximum values of segment joint opening widths for both crack models. Figures 12a-12d, 13d, 14a and 14b show that the maximum joint opening widths reduce from approximately 46 to 23 mm as the number of segments increases from 1 to 5. Formation of hairline flexural cracks along the beam axis is observed between the segment joints as well. These cracks and joint openings reduce the overall stiffness while they have insignificant effect on the ultimate load capacity (Figs. 11a and 11b). Segmental joint opening widths decrease with increasing number of segments for both crack models. The results showed that multi-segment beams had a greater ability to battle small width gaps under applied loads since the total expansion due to cracking is usually distributed among the segments. The observed data reveal that with each increment in the number of segments, an average reduction of approximately 8-10% occurs in the joint expansion. Notably, while this reduction ranges from 35 to 39 mm in the 2-segment beams, it fluctuates between 23 to 27 mm in the 5-segment beams.

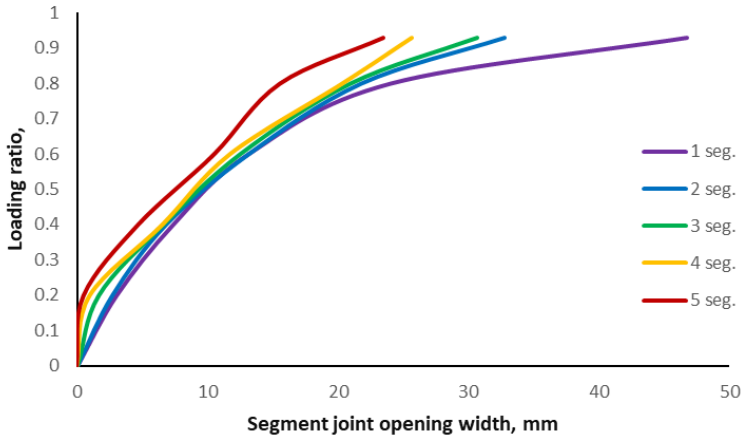

(a)

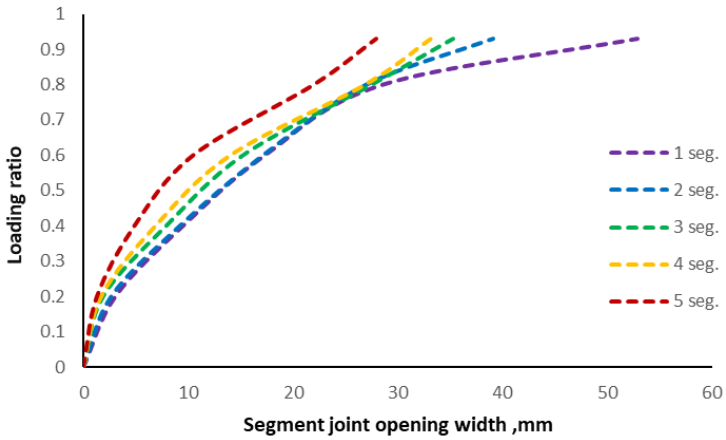

(b)

Fig. 14 Segment-joint opening width propagation graph up to collapse: (a) Rotating crack model and (b) Fixed crack model

Table 4 illustrates the relationship between the loading ratio and the corresponding segment opening width for different configurations of segmental beams, ranging from 2 segments to 5 segments. As the loading ratio increases from 0.25 to 1, the segment opening width generally exhibits a corresponding increase across all beam configurations. This indicates that higher loading ratios lead to greater deformation and widening of the segmental joints. Furthermore, it can be observed that as the number of segments increases, the segment opening width tends to decrease for a given loading ratio. This suggests that the presence of additional segments distributes the load more effectively, resulting in reduced deformation at the segmental joints.

Table 4. Loading ratio and segmental joint relationship in the segmental beams

Loading ratio	Segment opening width, mm			
	2-segment beam	3-segment beam	4-segment beam	5-segment beam
0.25	3.02	2.13	1.06	0.38
0.50	10.23	9.5	8.34	6.27
0.75	19.64	18.95	17.86	14.93
1	34,89	31.,24	25.68	23.12

4.3. Concrete Compressive Strength

In the parametric study, the compressive strength of concrete was assumed constant (40 MPa) in order to investigate the effect of the segment number on the load displacement and segment joint opening behavior. Thus, the effect of concrete compressive strength on load displacement, shear capacity, and joint opening width is evaluated for different concrete strengths ranging from 20 to 100 MPa for the beam with 5 segments. The analysis

results indicate that despite the asymptotical increase in moment capacity of the cross-section to almost 5200 kNm, the shear and joint shear capacity increases almost linearly with increasing concrete strength (Fig. 15). It should be mentioned herein that, for all concrete strength values, the shear capacity of segmental joints is shown to exceed the shear capacity of the cross-section. A similar observation can be made upon comparing the load displacement response of the beams given in Figure 16 concerning the almost linear initial stiffness and strength enhancement with increasing concrete strength while sustaining similar ductility level.

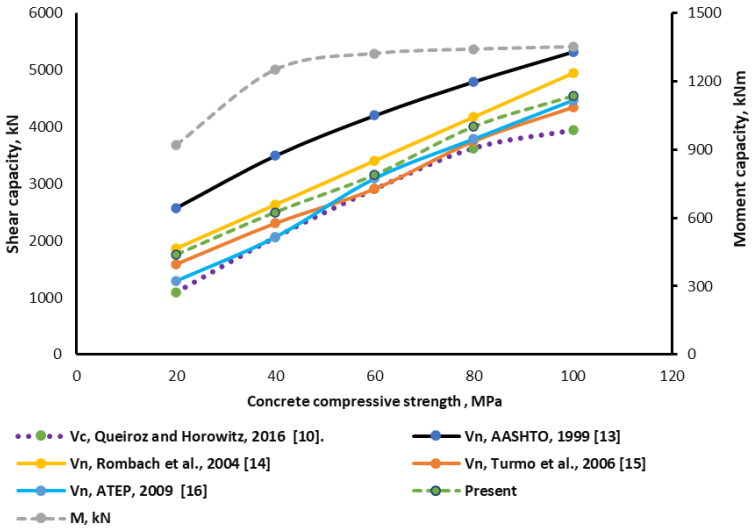

Fig. 15 Section and joint capacities changing according to concrete compressive strength

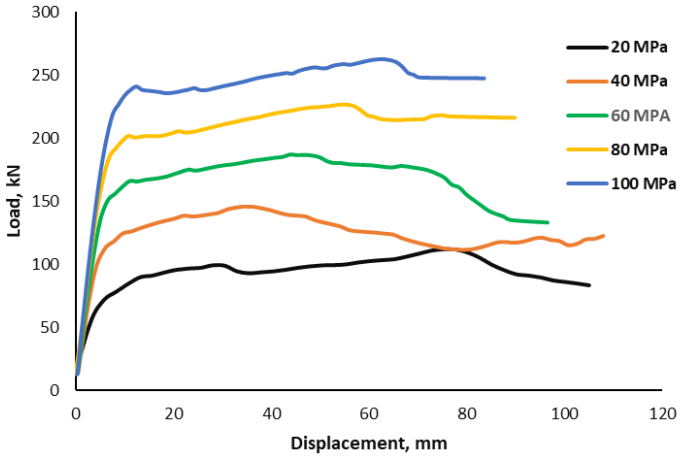

Fig. 16. Load–displacement curve of post tensioned circular hollow segmental beam

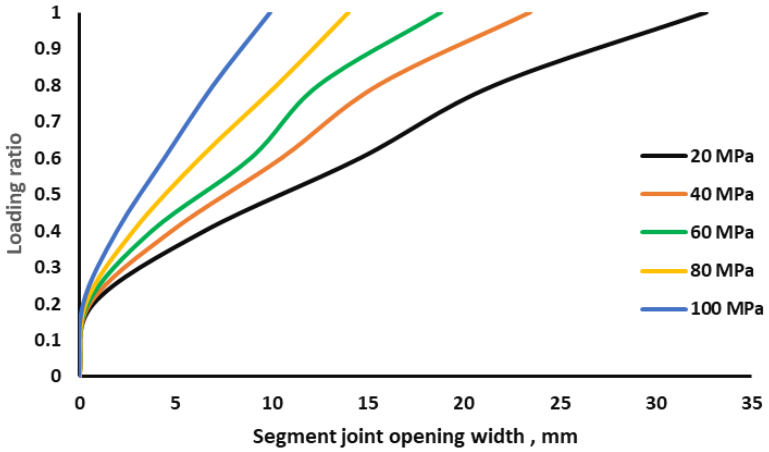

(a)

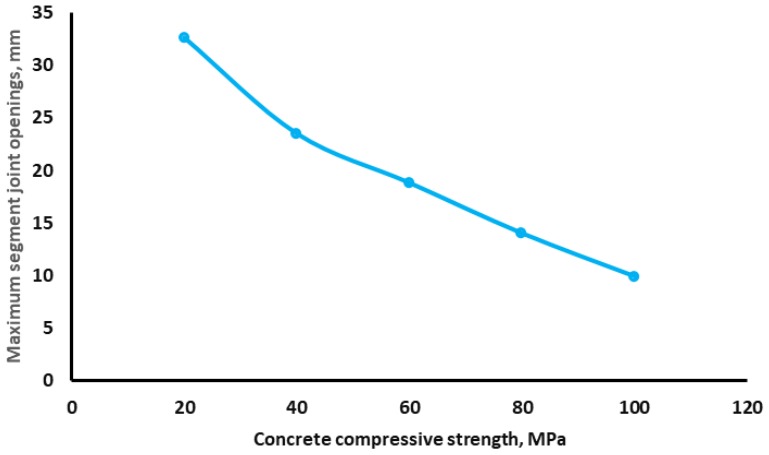

(b)

Fig. 17. Segmental joint opening for each concrete compressive strength in 5 - segment beam: (a) Segmental joint opening propagation (b) Maximum values of segment joint openings

Further, it is shown in Figures 17a that the maximum joint opening width tend to reduce with increasing concrete strength for each load level which are normalized according to the crack width at failure. For instance, when the compressive strength was 20 MPa, the segment joint opening width at collapse is 32.62 mm, whereas with the use of 100 MPa strength concrete, this value decreases substantially to 9.92 mm. (Fig. 17b).

5. Conclusion

In this study, the nonlinear structural behavior of hollow circular segmental post-tensioned (SPT) beams under 4-point bending is investigated. A scaled prototype structure is analyzed using DIANA FE software. 3 sets of verification problems are solved, and comparisons are made with the experimental results presented in the related studies. It is shown by the verification study conducted that it is possible to create accurate FE models for RC, PT and SPT beams using the selected software. The crack patterns obtained using the FE models are found out to be in excellent agreement with the experimentally obtained

patterns found in the cited studies. The numerical results obtained for the verification problems also show that a 3D FE model is required to model the scaled prototype structure since the complicated geometry of the intersegmental joints is required to be modeled using joint interface modeling technique. Increasing number of segments is found out to have a trivial effect on the load capacity of the segmental beams while reducing the intersegmental joint opening widths. The observed diminishing trend of the intersegmental joint opening widths with increasing number of segments and concrete strength indicates the potential benefits of utilizing more segments with high strength concrete. Analyses conducted on concretes with varying compressive strength levels underscore the effectiveness of the segmental design approach in various facets of offshore structures that already employ high compressive capacity concrete. The utilization of high compressive capacity concretes leads to minimal segment openings even under collapse conditions. In the structural design of such installations, the segmental methodology, which provides advantages in terms of both durability and ductility, can be regarded as a favorable option. Thus, it can be emphasized that, segmental construction is a viable option as long as the shear capacity and the opening width of intersegmental joints do not exceed code specified limits.

Furthermore, it is imperative to acknowledge certain limitations and provide avenues for future research to further enhance the understanding of segmental beam structures. Despite the comprehensive investigation conducted in this study, several limitations merit attention and offer potential directions for future exploration. One limitation lies in the scope of the study, which primarily focuses on the nonlinear structural behavior of hollow circular segmental post-tensioned (SPT) beams under 4-point bending. While this provides valuable insights into the behavior of segmental structures, future research could expand the scope to include additional loading conditions or investigate other structural configurations to provide a more comprehensive understanding of segmental beam behavior under diverse scenarios. Additionally, while the FE models employed in this study have demonstrated accuracy in capturing the structural response of RC, PT, and SPT beams, it is important to note that the modeling assumptions and simplifications inherent in the numerical analysis may introduce some degree of uncertainty. Future studies could explore alternative modeling approaches or validate the findings using experimental testing to enhance the robustness of the results. The study primarily focuses on the structural performance of segmental beams, neglecting other important aspects such as construction feasibility, cost-effectiveness, and environmental sustainability. Future research endeavors could incorporate these factors into the analysis to provide a more holistic assessment of segmental construction methodologies. In terms of future research directions, one potential avenue could involve investigating the long-term durability and resilience of segmental structures, particularly in harsh marine environments where offshore installations are prevalent. Additionally, exploring innovative construction techniques or material advancements could offer opportunities to further optimize the design and performance of segmental beam structures. By addressing these limitations and exploring new research directions, the field can continue to advance and refine segmental construction methodologies, ultimately enhancing the safety, efficiency, and sustainability of offshore structures.

Nomenclature

$1D$ = One dimensional.
$2D$ = Two dimensional;
$3D$ = Three dimensional;
FE = Finite Element;
RC = Reinforced Concrete;

PT = Post-tensioned;
SPT = Segmental post-tensioned;
k_n = Normal stiffnes;
k_t = Shear stiffnes;
t_n = Normal tractions;
t_t = Shear tractions;
u_n = Normal relative displacement;
u_t = Shear relative displacement;
E = Concrete elasticity modulus;
G = Concrete shear modulus;
t = Width of the interface;
$E_{ep.}$ = Epoxy elasticity modulus;
$G_{ep.}$ = Epoxy shear modulus;
μ_1 & μ_2 = Friction coefficients;
c = Cohesion;
M = Bending moment;
V = Shear force;
q = Distributed Load;
P = Point Load;
L = Length of beam
V_c = Circular hollow beam shear capacity;
α_{w2} = Reduction factor of concrete design resistance;
α_{cv} = Coefficient for deterimental effects on web crushing of high normal stresses;
f_{cd} = Design compressive strength of concrete ;
b_w = Effective web width;
D = External diameter of the cross section;
d = Depth of the cross section.
V_n = Nominal shear capacity of keyed dry joint;
A_k = Area of the base of all keys in the joint plane;
A_{sm} = Area of contact between smooth surfaces in the joint plane.
σ_n = Compressive stress in the joint.
f_{ck} = concrete characteristic compressive strength
A_j = Area of joint plane
f_{ym} =Yielding strength
f_{um} =Ultimate strength
ε_{su} = Ultimate strain
f_c = Concrete compressive strength
f_t = Concrete tensile strength
ρ = Concrete density
D = Diameter of longitudinal bar
d = Diameter of hooped bar
D_f = Diameter of tendon
ν = Poisson's ratio

Acknowledgement

This article was made possible with the support of the "Türkiye Burslari" supported by the "Presidency for Turks Abroad and Related Communities."

References

[1] Prestressed Concrete Institute (US). Committee on Segmental Construction. Recommended Practice for Segmental Construction in Prestressed Concrete. PCI. (1975).

[2] Liu, Wenbo, et al. Creep characteristics and time-dependent creep model of tunnel lining structure concrete. Mechanics of Time-Dependent Materials, 2021, 25: 365-382.https://doi.org/10.1007/s11043-020-09449-x

[3] LIU, X., Sun, Q., Song, W., & Bao, Y. Numerical modeling and parametric study of hybrid fiber-rebar reinforced concrete tunnel linings. Engineering Structures. 2022;251:113565. https://doi.org/10.1016/j.engstruct.2021.113565

[4] Zhang, W., Qiu, J., Zhao, C., Liu, X., & Huang, Q. Structural performance of corroded precast concrete tunnel lining. Tunnelling and Underground Space Technology. 2022;128:104658. https://doi.org/10.1016/j.tust.2022.104658

[5] Huang, Linchong, et al. Soil-water inrush induced shield tunnel lining damage and its stabilization: A case study. Tunnelling and Underground Space Technology, 2020, 97: 103290.https://doi.org/10.1016/j.tust.2020.103290

[6] Gong, C., Ding, W., Soga, K., & Mosalam, K. M. Failure mechanism of joint waterproofing in precast segmental tunnel linings. Tunnelling and Underground Space Technology. 2019;84:334-352. https://doi.org/10.1016/j.tust.2018.11.003

[7] Zhang, L., Feng, K., Gou, C., He, C., Liang, K., & Zhang, H. Failure tests and bearing performance of prototype segmental linings of shield tunnel under high water pressure. Tunnelling and Underground Space Technology. 2019;92:103053. https://doi.org/10.1016/j.tust.2019.103053

[8] Loth, E., Selig, M., & Moriarty, P. Morphing segmented wind turbine concept. In 28th AIAA Applied Aerodynamics Conf. 2010. https://doi.org/10.2514/6.2010-4400c

[9] Sobek, W., Plank, M., Frettlöhr, B., Röhm, J., & Corvez, D. Conceptual design of an UHPFRC tower structure in segmental construction for offshore wind turbines. In Proc. Of Int. Symposium on Ultra-High-Performance Fiber-Reinforced Conc. 2013; 423-432.

[10] Queiroz Junior, F. O., & Horowitz, B. Shear strength of hollow circular sections. Revista IBRACON de Estruturas e Materiais. 2016;9:214-225. https://doi.org/10.1590/S1983-41952016000200004

[11] CSA A23.3-04 Design of Concrete Structures. Standard CAN/CSA A23.3-04, Canadian Standards Association, Mississauga, Ont. 2004

[12] NBR 6118 Projeto de Estruturas de Concreto Procedimento, Associação Brasileira de Normas Técnicas Rio de Janeiro, RJ. 2014

[13] AASHTO. Guide Specifications for Design and Construction of Segmental Concrete Bridges. 1999. American Association of State Highway and Transportation Officials.

[14] Rombach, G. Dry joint behavior of hollow box girder segmental bridges. In Proceedings of the FIP Symposium. Segmental Construction in Concrete. 2004, New Delhi. http://hdl.handle.net/11420/7271

[15] Turmo, J., Ramos, G., & Aparicio, J. A. Shear strength of match cast dry joints of precast concrete segmental bridges: proposal for Eurocode 2. Materiales De Construcción. 2006;56(282):45–52. https://doi.org/10.3989/mc.2006.v56.i282.26

[16] ATEP. Proyecto y construcción de puentes y estructuras con pretensado ext. H.P.10-96. Colegio de Ing. De Caminos, Madrid. 1996.

[17] Pany, C. An insight on the estimation of wave propagation constants in an orthogonal grid of a simple line-supported periodic plate using a finite element mathematical model. Frontiers in Mechanical Engineering. 2022;8:926559. https://doi.org/10.3389/fmech.2022.926559

[18] Wegner, L. D., & Gibson, L. J. The fracture toughness behaviour of interpenetrating phase composites. International journal of mechanical sciences. 2001;43(8):1771-1791. https://doi.org/10.1016/S0020-7403(01)00016-9
[19] Puzrin, A. M., & Houlsby, G. T. Rate-dependent hyperplasticity with internal functions. Journal of engineering mechanics. 2003;129(3):252-263. https://doi.org/10.1061/(ASCE)0733-9399(2003)129:3(252)
[20] Pany, C., & Li, G. Application of periodic structure theory with finite element approach. Frontiers in Mechanical Engineering. 2023;9:1192657. https://doi.org/10.3389/fmech.2023.1192657
[21] Vamsi, A., ANSARİ, J., Sundaresan, M. K., Chitaranjan, P. A. N. Y., Bibin, J. O. H. N., Samridh, A., & Mercy, T. D. Structural design and testing of pouch cells. Journal of Energy Systems. 2021;5(2):80-91. http://dx.doi.org/10.30521/jes.815160
[22] Chitaranjan, P. A. N. Y. Investigation of Circular, Elliptical and Obround Shaped Vessels by Finite Element Method (FEM) Analysis under Internal Pressure Loading. Journal of Science, Technology and Engineering Research. 2022;3(1):24-31. DOI:10.53525/jster.1079858
[23] Pany, C. Estimation of Correct Long-Seam Mismatch Using FEA to Compare the Measured Strain in a Non-Destructive Testing of a Pressurant Tank: A Reverse Problem. International Journal of Smart Vehicles and Smart Transportation (IJSVST). 2021;4(1):16-28. https://doi.org/10.4018/ijsvst.2021010102
[24] Pany, C. Cylindrical shell pressure vessel profile variation footprint in strain comparison of test data with numerical analysis. Liquid and Gaseous Energy Resources. 2021;1(2):91-101. https://doi.org/10.21595/lger.2021.22163
[25] Jason, L., Torre-Casanova, A., Davenne, L. et al. Cracking behavior of reinforced concrete beams: experiment and simulations on the numerical influence of the steel-concrete bond. Int J Fract. 2013;180:243–260. https://doi.org/10.1007/s10704-013-9815-6
[26] Tao, X., & Du, G. Ultimate stress of unbonded tendons in partially prestressed concrete beams. PCI Journal. 1985;30(6):72-91.
[27] Al-Sherrawi, M. H., Allawi, A. A., Al-Bayati, B. H., Al Gharawi, M., & El-Zohairy, A. Behavior of precast prestressed concrete segmental beams. Civil Eng. J. 2018;4(3):488-496. http://dx.doi.org/10.28991/cej-0309109
[28] Ferreira, D., & Manie, J. DIANA —Finite Element Analysis: DIANA Documentation— Rel. 10.4. DIANA FEA BV. 2022.
[29] Ferreira, D. A model for the nonlinear, time-dependent and strengthening analysis of shear critical frame concrete structures. PhD Thesis, Univ. Pol. de Catalunya, Barcelona Tech. 2013. http://dx.doi.org/10.5821/dissertation-2117-94874
[30] Chai, S. Finite Element Analysis for Civil Engineering with DIANA Software. Springer Nature. 2020. https://doi.org/10.1007/978-981-15-2945-0
[31] MC90. CEB-FIP Model Code 1990. Bulletin d´Information No. 213/214, Comité Euro-International Du Béton. 1993.
[32] Kaya, S., & Salim, D. Shear Stiffness and Capacity of Joints Between Precast Wall Elements. Dissertation. 2017. Retrieved from https://urn.kb.se/resolve?urn=urn:nbn:se:kth:diva-209347
[33] Turmo, J., Ramos, G., and Aparicio, A.C. Study of the structural behaviour under flexure and shear of segmental concrete bridges with external prestressing and dry joints, Spain: ACHE. 2006.
[34] Červenka, V., Jendele, L. and Červenka, J. ATENA Program Documentation Part 1-Theory.Červenka Consulting s.r.o. 2016.
[35] Ramirez, G., MacGregor, R., Kreger, M. E., Roberts-Wollmann, C., Breen, J. Shear Strength of Segmental Structures. Proceedings of the Workshop AFPC External Prestressing in Structures. Saint-Remy-les-Chevreuse. 1993;pp. 287-296.